THE JOURNAL OF PHYSICAL CHEMISTRY B

ARTICLE

pubs.acs.org/JPCB

Modeling the Tetraphenylalanine-PEG Hybrid Amphiphile: From DFT Calculations on the Peptide to Molecular Dynamics Simulations on the Conjugate

David Zanuy,[†] Ian W. Hamley,[‡] and Carlos Alemán*[,†,§]

[†]Departament d'Enginyeria Química, E. T. S. d'Enginyeria Industrial de Barcelona, Universitat Politècnica de Catalunya, Diagonal 647, 08028 Barcelona, Spain.

[‡]School of Chemistry, Food Science and Pharmacy, University of Reading, Whiteknights, Reading RG6 6AD, United Kingdom

[§]Center for Research in Nano-Engineering, Universitat Politècnica de Catalunya, Campus Sud, Edifici C′, C/Pasqual i Vila s/n, Barcelona E-08028, Spain

ABSTRACT: The conformational properties of the hybrid amphiphile formed by the conjugation of a hydrophobic peptide with four phenylalanine (Phe) residues and hydrophilic poly(ethylene glycol), have been investigated using quantum mechanical calculations and atomistic molecular dynamics simulations. The intrinsic conformational preferences of the peptide were examined using the building−up search procedure combined with B3LYP/6-31G(d) geometry optimizations, which led to the identification of 78, 78, and 92 minimum energy structures for the peptides containing one, two, and four Phe residues. These peptides tend to adopt regular organizations involving turn-like motifs that define ribbon or helical-like arrangements. Furthermore, calculations indicate that backbone···side chain interactions involving the N−H of the amide groups and the π clouds of the aromatic rings play a crucial role in Phe-containing peptides. On the other hand, MD simulations on the complete amphiphile in aqueous solution showed that the polymer fragment rapidly unfolds maximizing the contacts with the polar solvent, even though the hydrophobic peptide reduce the number of waters of hydration with respect to an individual polymer chain of equivalent molecular weight. In spite of the small effect of the peptide in the hydrodynamic properties of the polymer, we conclude that the two counterparts of the amphiphile tend to organize as independent modules.

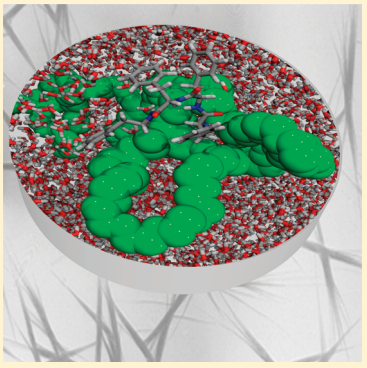

INTRODUCTION

The design of hybrid materials, i.e., molecular architectures based on combining naturally occurring molecular segments and synthetic entities, is a rapidly growing field within materials science due to advanced applications from the combination of each counterpart properties.[1,2] Among them, peptide-containing amphiphiles have recently focused special attention since they combine the specificity of peptide interactions (for instance, targeted binding to proteins) with properties inherent to amphiphiles such as the capacity to self-assemble into complex ordered aggregates, which can range from micelles to nanofibrils.[3−5] Thus, systems based on fragments of the amyloid beta peptide (hereafter named Aβ) present a high propensity to form fibrils (e.g., the KLVFF segment, which is part of its hydrophobic core from residues 16 to 20, has been identified as one of the key sequences for the fibrillization of the full Aβ peptide[6]).

Recently a new hybrid material was obtained by conjugating the FFKLVFF peptide, which is Aβ(16−20), KLVFF, extended by two phenylalanine (Phe) residues, with the highly hydrophilic poly(ethylene glycol), hereafter abbreviated PEG.[7] While FFKLVFF is highly hydrophobic and does not dissolve in water (it form fibers in methanol[8]), its conjugation with PEG leads to an amphiphilic molecule which forms self-assembled fibrillar structures in dilute aqueous solution and nematic and hexagonal columnar liquid crystal phases at higher concentration.[9−11]

The presence of a charged residue in the amyloidogenic core of the peptide segment precluded the complete understanding of which residues held the key of the association process. In an effort to understand the role of different intermolecular interactions in the self-assembly, a new hybrid sytem was prepared by combining PEG with a peptide comprising four consecutive Phe residues, i.e., FFFF-PEG.[12] The lack of charged or polar residues in the peptide sequence renders FFFF-PEG an ideal model system comprising a short but very hydrophobic peptide moiety. Moreover, conjugation of PEG conferred amphiphilic properties to the new material enabling self-assembly in aqueous solutions.[12] Moreover, PEG should improve the applicability of this material since it is well established that this polymer is an excellent steric stabilizer, which helps to encapsulate insoluble small molecules such as drugs, prevents or hinders their uptake, and facilitates their slow release. Experimental results revealed that FFFF-PEG tends to aggregate via hydrophobic interactions, even at moderately

Received: April 4, 2011
Revised: June 9, 2011
Published: June 14, 2011

low concentrations, with a characteristic critical aggregation concentration. Above it, β-sheet organizations are detectable even before straight fibril structures start growing and depositing. These aggregates are much shorter than those observed for amyloid peptides though. Finally, PEG crystallization does not disrupt local β-sheet structure, even though on longer length scales the β-sheet fibrillar structure might be perturbed by the formation of spherulites from PEG crystallization.[12]

In this work we examine the intrinsic conformational properties of the FFFF segment and how its conjugation with PEG affects the conformational preferences of both the hydrophobic peptide and the inner hydrodynamic properties of the polymer. Initially, the intrinsic conformational preferences of homopeptides containing 1, 2, and 4 Phe residues have been characterized, combining the build-up search procedure with quantum mechanical calculations. After this, atomistic molecular dynamics (MD) simulations of the FFFF-PEG hybrid system have been carried out in aqueous solution. Results provide an atomistic characterization of the intrinsic conformational properties of both the peptide and the complete conjugate.

METHODS

Conformational Studies on Tetra-Phenylalanine. *Building-Up Strategy.* The intrinsic conformational preferences of the isolated tetrapeptide Ac-$(Phe)_4$-NHMe, where Ac and NHMe refer to acetyl and *N*-methylamide, respectively, were investigated using density functional theory (DFT) quantum mechanical calculations. A modified build-up scheme was used to assess the effect of the peptide length over the Phe conformational properties. The building-up approach is based on the assumption that short-range interactions play a dominant role in determining the conformation of any given polymeric system.[13] For a given polymer, the accessible conformations result from the combination of *N* independent rotamers (i.e., the rotational isomeric approximation[14]), in which each independent rotational state corresponds to the most favored conformations of each repetitive unit. The practical application of this approach imposes that, after exhaustive conformational analyses of small fragments of the studied model, only those local minima with relative energies within a selected threshold are retained to form selected sets of minima. The selected set of minima of one fragment is then combined with the selected set of another fragment, providing new starting points of the longer fragment for geometry optimization. In our case, due to the peptide sequence symmetry (i.e., four identical Phe residues), the fragment first studied was the Ac-Phe-NHMe dipeptide (hereafter referred to as *F*), followed by the Ac-$(Phe)_2$-NHMe tripeptide (F_2) as a combination of two *F* fragments. Finally, Ac-$(Phe)_4$-NHMe (F_4) was built by combining two F_2 tripeptide minima.

The conformational preferences of the *F* dipeptide were explored by combining all theoretical minima of each dihedral angle with free rotation present in the Phe residue (Figure 1a). Hence, two torsions correspond to the main chain conformational freedom (φ,ψ), while the other two drive the geometrical disposition of the side chain (χ_1,χ_2). Each of these torsions is expected to exhibit three theoretical positions of low energy (gauche$^+$, trans, and gauche$^-$), which leads to 3 (φ) × 3 (ψ) × 3 (χ_1) × 3 (χ_2) = 81 starting structures for the conformational search of *F*. Finally, the peptide bonds at the N and C termini were assumed to present a conventional trans arrangement, which is the most favored.[15−17]

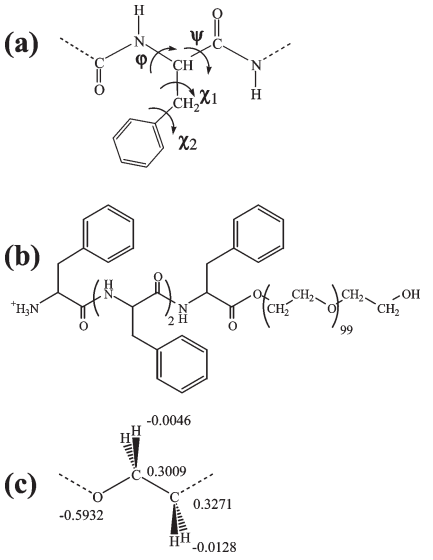

Figure 1. (a) Schematic representation of the Phe building block. The backbone and side-chain dihedral angles are indicated. (b) Schematic representation of the studied hybrid molecule. (c) Electrostatic parameters determined for the repeating units of the PEG chain.

Among all of the structures obtained for *F*, 10 different conformations within a relative energy threshold of 5.0 kcal/mol with respect to the absolute minimum were selected for the combinatorial process of the next building-up step. Hence, each of such conformations was combined with the other nine and with itself, leading to 100 new starting structures for F_2. For each of these structures the effect of the side chain flexibility over the growing molecule was explicitly studied using the approach proposed by Gibson and Scheraga.[13] First, the new molecule was built as an alanine (Ala) tripeptide (A_2), and the dihedral angles of its backbone conformation were fixed to those resulting from the combination of the above selected minima. The first side chain of this initial system (i.e., a methyl group) was then replaced by the side group of Phe. A complete exploration was performed for the new side group considering the 3 (χ_1) × 3 (χ_2) = 9 theoretical energy minima, but keeping the backbone dihedral angles fixed. The lowest energy conformation for the side chain of the first Phe residue was kept for the next step. Then, the same strategy was used for the second Phe residue. Finally, the most stable side chain arrangement was used as starting point for complete geometry optimization of the initial backbone conformation.

Finally, the exploration of the most favored organizations for F_4 was completed by combining the minima of two F_2 fragments. In this case though, the relative energy threshold for selected F_2 arrangements was reduced to 3.0 kcal/mol, which led to the combination of 10 × 10 = 100 initial structures. The effect of the side chain on the growing peptide was studied for each structure of F_4 using the approach discussed above for F_2. Thus, the side chains of the Phe residues were independently optimized from residue one to four, while the backbone conformation was kept fixed, the most stable side chain being used as starting point for complete geometry optimization.

Conformational Characterization. The optimized structures of *F*, F_2, and F_4 were characterized according to the conformations of both the backbone and the side chains. Backbone conformations were categorized using the nomenclature proposed by Perczel and co-workers.[18] This procedure distributes the

potential energy surface $E = E(\varphi,\psi)$ of α-amino acids in nine different regions: γ_D, δ_D, α_D, ε_D, β_{DL}, ε_L, α_L, δ_L, and γ_L. On the other hand, the arrangements of the side chains were labeled according to the conformations adopted by the dihedral angles χ_1 and χ_2. Specifically, each rotamer was classified as gauche, skew, trans, or cis. Due to the inner symmetry the phenyl ring, the degenerated conformational states, gauche$^+$/gauche$^-$ and skew$^+$/skew$^-$, have been computed as unique and equivalent orientations.

Clustering of Structures: Conformational Classification. A list of unique minimum energy conformations was constructed by assessing the similarities among the different structures. This was performed by applying a geometric criterion that was successfully used in previous works to describe the conformational preferences of small peptides.[19−22] Specifically, virtual dihedral angles were defined for F_2 and F_4 considering the α-carbon atoms of each residue, the methyl carbon atom of the Ac and NHMe capping groups. The aforementioned list was organized by rank, ordering all of the unique minimum energy conformations found following an increasing order of energy. Two conformations were considered different if they differ in at least one of their virtual dihedral angles by more than 60°. The same procedure was applied for F but considering the dihedral angles φ and ψ.

Computational Details. Calculations on the three Phe-containing peptides derivates were carried out by combining the B3LYP functional[23,24] with the 6-31G(d) basis set.[25] All calculations performed using the Gaussian 03 computer program.[26]

Amphiphile FFFF-PEG. *Molecular Models.* The conformational properties of FFFF-PEG were studied using MD simulations. The molecular model consisted of a PEG chain containing 100 repeating units bound to a peptide formed by four Phe residues (Figure 1b). The difference between the latter and F_4 is that the N-terminus is unprotected in the amphiphile (i.e., it involves an ionized amino group as would be observed at neutral pH). The C-terminus of the peptide main chain is linked to the polymer moiety by an ester bond. The last repeating unit of PEG was terminated with a hydroxyl group. The starting conformation for the polymeric segment was modeled using an stochastic methodology.[27,28] The hybrid molecule was placed in the center of a cubic simulation box (a = 90 Å) filled with 19935 explicit water molecules, which were represented using the TIP3 model.[29] One chloride ion was added to the simulation box to reach electric neutrality.

Potential Energy Computation. The potential energy of the simulated system was computed using the Amber force field.[30] All of the parameters for the peptide were extracted from Amber libraries,[30] whereas bonding and van der Waals parameters for PEG were extrapolated from the GAFF forcefield,[31] using as reference those previously published for force fields type I.[32,33] Electrostatic parameters for PEG were specifically developed in this work using a model compound with three repeating units. Specifically, atomic centered charges were obtained by fitting the molecular electrostatic potentials (MEPs) calculated using a large set of points placed outside the nuclear region at the HF/6-31G(d) quantum mechanical and the Coulombic classical levels (Figure 1c). The electrostatic parameters derived using such a procedure are fully compatible with the current parameters of the AMBER force-field.[34]

Simulation Details. MD simulations were performed using the NAMD program.[35] Atom pair distance cut-offs were applied at 14.0 Å to compute the van der Waals and electrostatic interactions. In order to avoid discontinuities in the potential energy function, nonbonding energy terms were forced to slowly converge to zero by applying a smoothing factor from a distance of 12.0 Å. Both temperature and pressure were controlled by the weak coupling method, the Berendsen thermobarostat,[36] using a time constant for heat bath coupling and a pressure relaxation time of 1 ps. Bond lengths were constrained using the SHAKE algorithm[37] with a numerical integration step of 2 fs.

Before starting the MD run series, 5×10^3 steps of energy minimization were performed to relax conformational and structural tensions. Then, the system was heated and equilibrated by a series of consecutive MD runs. Thus, 0.5 ns of NVT-MD at 500 K were used to homogeneously distribute the solvent and ion in the box. Next, thermal equilibration for 0.5 ns in the constant-NVT ensemble at 298 K, and a density relaxation for 0.5 ns in the constant-NPT ensemble at 298 K were performed. The last snapshot of the NPT-MD was used as the starting point for the production series. Coordinates were saved every 2 ps for further analysis for simulation length of 20 ns.

Table 1. Relative Energy (ΔE in kcal/mol), Backbone Conformation According to the Nomenclature Proposed by Perczel et al.,[18] Secondary Structure Associated with the Backbone Conformation, Side Chain Conformation According to χ_1 and χ_2, and Intramolecular Interactions (Both Hydrogen Bonds and N−H···π) of the Structures Calculated for F at the B3LYP/6-31G(d) Level[a]

no.	ΔE	backbone	motif	χ_1[b]	χ_2[b]	H bond[c]	N−H···π[d]
I	0.0[d]	γ_L	γ-turn	gauche	skew	C_7	Phe···π
II	0.7	β_{DL}	fully extended	trans	gauche	C_5	NHMe···π
III	0.8	γ_L	γ-turn	trans	gauche	C_7	
IV	1.0	γ_L	γ-turn	gauche	skew	C_7	
V	2.11	α_L	helical	gauche	skew		Phe···π
VI	2.6	γ_D	reverse γ-turn	gauche	skew	C_7	Phe···π
VII	3.0	β_{DL}	fully extended	gauche	gauche	C_5	
VIII	3.9	β_{DL}	fully extended	gauche	skew	C_5	
IX	4.1	γ_L	γ-turn	gauche	gauche	C_7	Phe···π
X	4.5	γ_D	reverse γ-turn	trans	gauche	C_7	

[a] Only the structures with ΔE < 5.0 kcal/mol have been included. [b] Conformations have been categorized according to the trans, skew, and gauche rotamers (see Methods section). [c] C_7 and C_5 refer to seven- and five-membered hydrogen bonding rings, respectively. Phe and NHMe indicates that the N−H bond of the Phe residue and the blocking group, respectively, is participating in the interaction. [d] E = −726.906133 au.

RESULTS AND DISCUSSION

Homopeptides of Phenylalanine. A total of 78 different structures were obtained for F out of 81 starting points, which clustered in 18 different conformations for the backbone. The conformational characteristics and relative energies (ΔE) of the structures with ΔE < 5.0 kcal/mol are displayed in Table 1. These results are very similar to those either previously reported using first principle calculations[38] or extracted from the analysis of the conformation adopted by Phe in crystallized proteins.[38] As it can be seen in Figure 2, the most favored conformations (i.e., those with ΔE < 2.5 kcal/mol) are located in a very small region of the Ramachandran plot, which includes three minima in the γ_L region (**I**, **III**, and **IV** in Table 1), one minimum energy structure in the β_{DL} region (**II** in Table 1) and one low energy structure close to the α_L region (**V** in Table 1). The γ_L and β_{DL} structures correspond to γ-turn and fully extended motifs, respectively,

dx.doi.org/10.1021/jp2031187 |J. Phys. Chem. B 2011, 115, 8937–8946

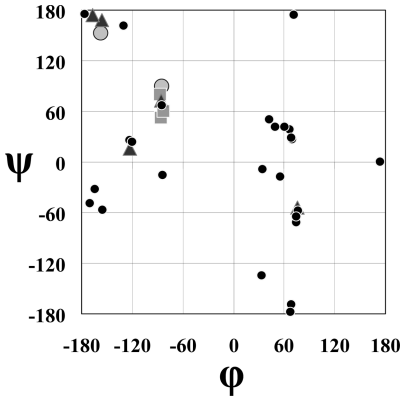

Figure 2. Distribution in the φ,ψ map of the structures obtained for the *F* dipeptide. The size and shape of the symbols have been used to represent the relative stability of the different structures. Specifically, large gray circles correspond to minima with $\Delta E < 1$ kcal/mol, large gray squares correspond to structures with 1 kcal/mol $\leq \Delta E < 2$ kcal/mol, black smaller triangles to structures with 2 kcal/mol $\leq \Delta E < 3$ kcal/mol and small rhomboids to the arrangements with $\Delta E > 3$ kcal/mol.

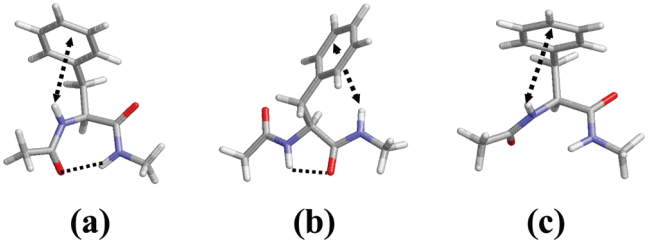

Figure 3. Minimum energy conformations calculated for *F* at the B3LYP/6-31G(d) level: (a) **I**, (b) **II**, and (c) **V**. The labels used to identify the different minima are described in the text. Intramolecular interactions defining seven- and five-membred hydrogen bonding rings (dashed lines) and N−H···π interactions (dashed arrows) are indicated.

presenting intramolecular seven- and five-membered hydrogen bonding rings, while the α_L structure shows a distorted helical conformation.

The ΔE values listed in Table 1 are strongly influenced by the existence of intramolecular interactions between the aromatic moiety of the side group and the NH of the backbone amide groups. This is illustrated in Figure 3a, which represents the lowest energy structure of *F*. This conformation shows two intramolecular interactions: the backbone···backbone hydrogen bond typically found in γ-turn motifs and N−H···π interaction between the π cloud of the phenyl ring and the N−H of the Phe residue. Similarly, the five membered hydrogen bonded ring of **II** is accompanied by the N−H···π backbone···side chain interaction (Figure 3b), even though in this case the N−H belongs to the NHMe blocking group. The energy gap between the γ_L and β_{DL} conformations calculated for the blocked Ala dipeptide is larger than 1.5 kcal/mol, whereas ΔE reduces to 0.7 kcal/mol for *F* (Table 1). The N−H···π interaction also expands its influence to the helical α_L structure of *F* (**V** in Table 1), which is represented in Figure 3c. Thus, the destabilization of this structure with respect to the γ_L conformer is 5.0 and 2.1 kcal/mol for the Ala and Phe dipeptides, respectively. It should be mentioned that the remarkable impact of the N−H···π interactions on the conformational preferences were

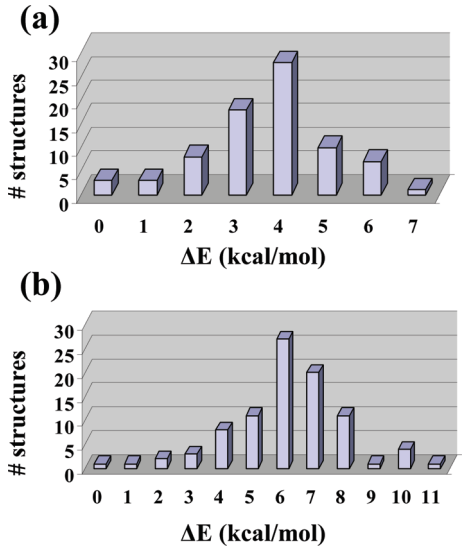

Figure 4. Distribution of energies for the minimum energy structures calculated using quantum mechanical calculations at the B3LYP/6-31G(d) level for (a) F_2 and (b) F_4.

previously reported for other small dipeptides containing aromatic side groups.[39−41]

The combinatorial growth of the peptide chain by considering the ten arrangements with $\Delta E < 5.0$ kcal/mol obtained for *F* provided 100 initial geometrical arrangements for F_2 that converged over a total of 78 minimum energy structures. The distribution of the energies associated with these minima fits a Gaussian function (Figure 4a), as is expected for the density of states provided by the rotational isomeric approximation with the assumption that the molecule is composed of *N* independent rotamers.[14] Clustering analysis converged the 78 minimized structures into 20 different conformations, which expanded within a ΔE interval of 7.3 kcal/mol. Table 2 lists the relative energy of the most stable conformation of each cluster for all the clusters with $\Delta E < 3.0$ kcal/mol (i.e., the rest of conformations of each cluster have been excluded because they are less favored organizations of the same basic structural motif), the conformational characteristics of the backbone, which are identical for all the conformations of a given cluster, and the conformational characteristics of the side groups in terms of distributions (i.e., populations for each dihedral angle were determined by considering the two Phe residues of all the conformations belonging to the same cluster).

Among the 20 basic organizations, the conformation that presented the lowest energy, **Id** where d refers to dimer (Figure 5a), corresponds to a double γ-turn (also denoted 2.2_7 ribbon), which is the outcome of replicating the most favored arrangement of *F* (structure **I** in Table 1). This regular organization has only been observed in short peptides.[42] As it can be seen, structure **Id** is stabilized by a network of intra- and inter-residue noncovalent interactions that include two backbone···backbone hydrogen bonds and one backbone···side chain N−H···π interaction. The three following structures **IId**, **IIId**, and **IVd** are irregular organizations in which each Phe adopts a different organization. Side chains tend to adopt conformations suitable to set N−H··· π interactions with the peptide groups of the backbone, enhancing the stability of these structures. The low variability in the conformational preferences of the side chains

dx.doi.org/10.1021/jp2031187 |*J. Phys. Chem. B* 2011, 115, 8937–8946

Table 2. Relative Energy (ΔE in kcal/mol), Backbone Conformation for Every Phe Residue According to the Nomenclature Proposed by Perczel et al.,[18] and Averaged Populations Showing the Organization of the Side Groups (χ_1 and χ_2 Dihedral Angles) of the Structures Calculated for F_2 at the B3LYP/6-31G(d) Level[a]

		residue		χ_1				χ_2			
no.	ΔE	Phe1	Phe2	gauche	trans	skew	cis	gauche	trans	skew	cis
Id	0.0[b]	γ_L	γ_L	67	33	0	0	17	0	83	0
IId	0.1	γ_L	γ_L	100	0	0	0	50	0	50	0
IIId	0.7	β_{DL}	γ_L	25	75	0	0	25	0	75	0
IVd	1.1	δ_L	γ_L	75	25	0	0	50	0	50	0
Vd	1.8	β_{DL}	β_{DL}	33	33	33	0	0	0	100	0
VId	1.9	β_{DL}	δ_L	67	33	0	0	67	0	33	0
VIId	2.2	β_{DL}	γ_L	75	25	0	0	0	0	100	0
VIIId	2.4	γ_L	γ_D	67	33	0	0	17	0	83	0
IXd	2.5	γ_D	γ_L	75	25	0	0	0	0	100	0
Xd	2.7	α_L	γ_L	100	0	0	0	50	0	50	0

[a] Only the structures with ΔE < 3.0 kcal/mol have been included. [b] E = −1205.286460 au.

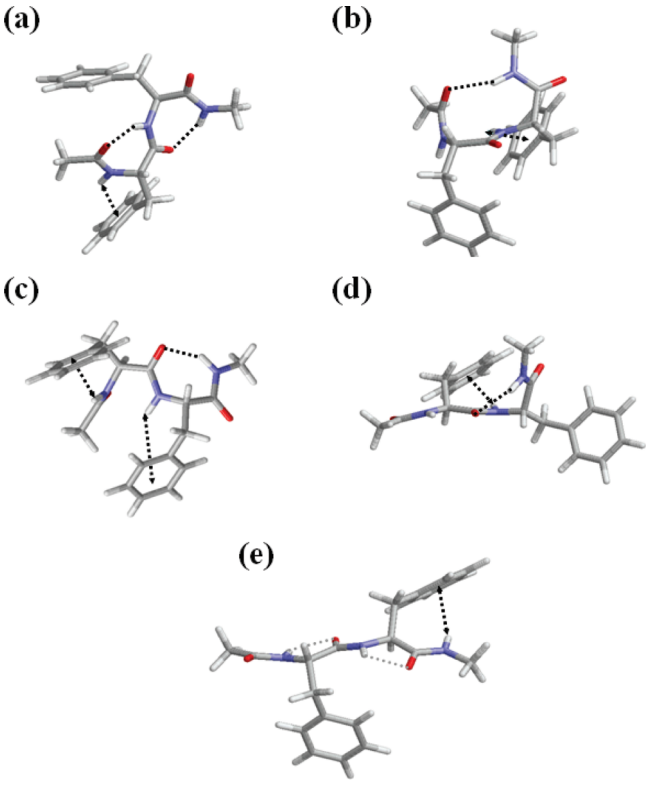

Figure 5. Minimum energy conformations calculated for F_2 at the B3LYP/6-31G(d) level: (a) **Id**, (b) **IId**, (c) **IIId**, (d) **IV**, and (e) **Vd**. The labels used to identify the different minima are described in the text. Intramolecular interactions defining seven- and five-membred hydrogen bonding rings (dashed black lines and gray dotted lines, respectively) and N−H···π interactions (dashed arrows) are indicated.

corroborates the previous observation. Among the most favored structures, the preferred arrangement for χ_1 is gauche followed by trans, whereas χ_2 shows almost always folded conformations, either skew or gauche.

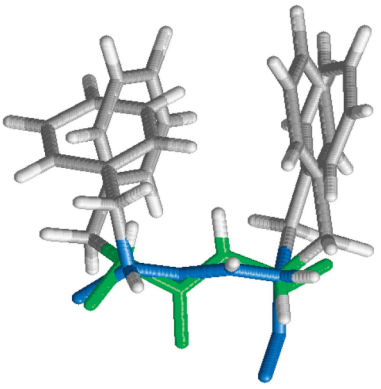

Figure 6. Superposition of the conformation adopted by the unblocked Phe−Phe peptide (blue) in the solid state and the closest minimum energy conformation calculated for F_2 (green).

Structure **IId** (Figure 5b) represents a folded structure that is the outcome of forming an intramolecular hydrogen bond between the C═O and NH moieties of the Ac and NHMe blocking groups, respectively. This particular arrangement may be associated to a β-turn motif or to an embryonic helical organization that would render a 3_{10} helix if the peptide could be prolonged beyond the two residues of Phe. Structure **IIId** (Figure 5c), which results from the combination of distorted extended β_{DL} and γ-turn motifs, presents two N−H···π intraresidue interactions. Structure **IVd** (Figure 5d) shows a hydrogen bond associated to the γ-turn motif of the second Phe residue and an inter-residue N−H···π interaction. The change in the side chain···backbone interaction pattern with respect to **IIId** produces a destabilization of 0.4 kcal/mol, indicating that the conformational preferences of F_2 are very dependent on a delicate energetic balance between all possible interacting groups.

On the other hand, structure **Vd** corresponds to a completely extended arrangement that is built upon the combination of two β_{DL} conformations (Figure 5e). This arrangement is disfavored by 1.8 kcal/mol with respect to the lowest energy structure and is the basis for the formation of self-assembled complexes of Phe-containing oligomers both as free independent peptides[43] and as parts of hybrid amphiphile chains.[12] The following two minima (**VId** and **VIId**) are the combination of the β_{DL} conformation in the first Phe residue with a folded pattern in the second Phe residue, whereas **VIIId** and **IXd** are the two possible organizations resulting from the γ_L and γ_D conformations. Finally, the last structure listed in Table 2 corresponds again to an incipient helical organization, in which the ten-membered hydrogen bonded ring is partially distorted by the conformation of the second residue side chain.

The crystal structure of the unblocked Phe-Phe peptide (i.e., the F_2 analogue in which the Ac and NHMe blocking groups are replaced by hydrogen atoms) was reported by Görbitz one decade ago.[44] This author found that this small peptide crystallizes with hydrogen bonded head-to-tail chains forming hydrophilic channels embedded in a hydrophobic matrix created by the peptide side chains. Indeed, the sequence formed by two consecutive Phe residues was proposed to be an attractive model for membrane channels due to the substantial size of the hydrophilic channels. Interestingly, the conformation adopted by the unblocked peptide in the solid state has been identified in the current study as a minimum energy conformation. The resemblance

dx.doi.org/10.1021/jp2031187 |J. Phys. Chem. B 2011, 115, 8937–8946

Table 3. Relative Energy (ΔE in kcal/mol), Backbone Conformation for Every Phe Residue According to the Nomenclature Proposed by Perczel et al.,[18] and Averaged Populations Showing the Organization of the Side Groups (χ_1 and χ_2 Dihedral Angles) of the Structures Calculated for F_4 at the B3LYP/6-31G(d) Level[a]

		residue				χ_1				χ_2			
no.	ΔE	Phe1	Phe2	Phe3	Phe4	gauche	trans	skew	cis	gauche	trans	skew	cis
It	0.0[b]	γ_D	γ_L	γ_D	γ_L	100	0	0	0	0	0	75	25
IIt	0.7	γ_L	γ_L	γ_L	γ_L	100	0	0	0	0	0	0	100
IIIt	1.5	γ_L	γ_L	α_L	γ_L	100	0	0	0	25	0	50	25
IVt	2.0	γ_L	α_L	γ_D	γ_L	100	0	0	0	25	0	50	25
Vt	3.0	γ_L	γ_L	α_L	γ_L	100	0	0	0	38	0	38	24
VIt	3.0	γ_D	γ_L	α_L	γ_L	100	0	0	0	25	0	50	25
VIIt	3.5	γ_L	δ_L	γ_L	γ_L	100	0	0	0	12	0	63	25
VIIIt	4.0	γ_L	γ_L	γ_D	γ_L	100	0	0	0	12	0	63	25
IXt	4.5	γ_L	γ_L	γ_L	γ_L	80	20	0	0	30	0	45	25
Xt	4.9	β_{DL}	γ_D	α_L	γ_L	83	17	0	0	8	0	67	25
XIt	5.1	β_{DL}	γ_L	β_{DL}	γ_L	56	44	0	0	12	0	63	25
XIIt	5.2	β_{DL}	γ_L	β_{DL}	γ_L	38	50	12	0	12	0	63	25
XIIIt	5.3	γ_D	γ_L	γ_L	γ_L	92	8	0	0	0	0	75	25
XIVt	5.4	β_{DL}	γ_L	γ_L	β_{DL}	62	38	0	0	0	0	75	25
XVt	5.6	β_{DL}	γ_L	α_L	γ_L	75	25	0	0	25	0	50	25
XVIt	5.6	β_{DL}	γ_D	γ_L	γ_L	75	12	12	0	0	0	75	25
XVIIt	5.9	β_{DL}	γ_L	γ_L	β_{DL}	75	25	0	0	0	0	75	25
XVIIIt	5.9	γ_L	δ_L	γ_L	γ_L	88	12	0	0	25	0	50	25
IXt	6.0	β_{DL}	γ_L	β_{DL}	γ_L	40	60	0	0	10	0	65	25
XXt	6.0	β_{DL}	β_{DL}	β_{DL}	β_{DL}	11	86	3	0	17	0	78	5

[a] Only the structures with $\Delta E < 6.0$ kcal/mol have been included. [b] $E = -2162.052694$ au.

between the theoretically and experimentally determined conformations is evidenced in Figure 6, which shows a superposition of the two structures. This minimum, which is destabilized by 3.3 kcal/mol with respect to **Id**, is number thirteen in the list of unique conformations provided by the build-up procedure. However, such an energy penalty is easily compensated in the crystal through the formation of attractive intermolecular interactions.

The last building-up cycle provided the conformational preferences of F_4. The 100 initial structures, generated by the strategy previously described (Methods section), produced 92 different optimized geometries. The distribution of the energies associated with these minima again fits a Gaussian distribution (Figure 4b). Among those 92 structures, only 34 different arrangements were categorized as unique structural motifs within a ΔE interval that expanded up to 11.1 kcal/mol. As was already mentioned for F_2, these ΔE values correspond to the relative energy of the most stable arrangement for each clustered motif. The most favored conformational motifs for the studied Phe-tetramer are listed in Table 3. In this case the range of listed conformations was expanded according to the experimental evidence, which showed that Phe-containing oligomers tend to aggregate forming long sheets of β-strands.[12,40] In our conformational search, the totally extended arrangement (**XXt** structure in Table 3, where **t** refers to tetramer) was 6.0 kcal/mol less favored than the absolute minimum. Including structures up to that ΔE value could be considered an overestimation, because a Boltzmann distribution of populations would label any structure beyond ~2 kcal/mol totally improbable at room temperature. However, our studies did not include the effect of the solvent on the conformational preferences, nor did we examine cooperative effects that aggregation of strands could provide.

The scenario depicted by Table 3 clearly highlights the predominance of folded patterns in front of extended or partially extended conformations. In particular the predominant role of γ-turn motifs, combined in lesser amount with β-turns and pseudohelical arrangements, is the most remarkable feature for the nine first optimized structures. Among them, the symmetrical distribution of conformers is the most favored organization, even though those arrangements with lower symmetry are disfavored by energy differences that range between 1.5 and 2.5 kcal/mol, depending on the position of the residue that breaks the symmetry.

Structure **It** (Figure 7a) is an especially interesting case: even though the starting arrangement is the duplication of the ninth minimum detected for F_2 (**IXd** in Table 2), the final organization resembles a helical organization that already tends to overcome the hydrogen bonding pattern of multiple γ-turn motifs. Thus, the Ac and NHMe blocking groups form a hydrogen bond that closes a 14-membered ring. It is worth noting that this hydrogen bond pattern does not match with any secondary structure motif, and it is apparently due to the tight organization that four turn conformations of opposite symmetry imposes (i.e., reverse γ-turn for Phe1 and Ph3 and γ-turnPhe2 and Phe4). Finally, it is noticeable that this organization does not favor the formation of N−H$\cdots\pi$ interactions that were present in F_2 and that will reappear in other structures of the tetramer.

The organization of **IIt** (Figure 7b), which is the natural outcome of duplicating **Id** (Table 2), corresponds to a 2.2_7 ribbon. Actually, if the peculiar space distribution of interacting functional groups in **It** were to be disregarded as an exception, **IIt** would be the expected most stable organization. As can be seen in Figure 7b, the formation of an ideal ribbon secondary structure

provides the perfect arrangement to guarantee the maximization in the number of intramolecular interactions, even though in some cases their interaction geometries might not be as optimal as they could be expected. For example, the third backbone···backbone hydrogen bond diverges from the optimal values, enlarging the distance H···O to 2.36 Å and decreasing the ∠N−H···O angle down to 126.1°.

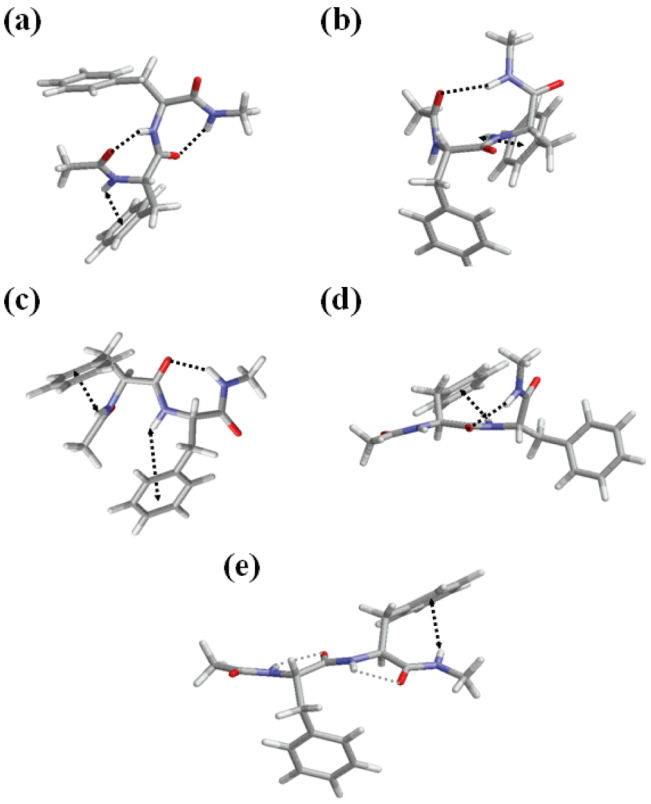

Figure 7. Minimum energy conformations for F_4 at the B3LYP/6-31G(d): (a) **It**, (b) **IIt**, (c) **IIIt**, (d) **IVt**, and (e) **Xt**. The labels used to identify the different minima are described in the text. Intramolecular interactions defining seven- and five-membered hydrogen bonding rings (dashed black lines and gray dotted lines, respectively) and N−H···π interactions (dashed arrows) are indicated.

The following 7 arrangements are combinations of γ-turns with other folded arrangements that compensate the loss of seven-membered hydrogen bonding pattern with the formation of other intramolecular interactions. The structures shown in Figure 7, panels c and d, are the combination of γ-turn−γ-turn (**IIIt**) and reverse γ-turn−γ-turn (**IVt**) motifs, respectively, with other arrangements. In both cases the folded segment enables the formation of a ten-membered hydrogen bonded ring, characteristic of β-turn and helix 3_{10}, and one N−H··· π interaction. Thus, the break of the main chain regularity is partially balanced by the formation of a helical-like conformation.

The following group of identified structures corresponds to those partially extended conformations. These arrangements appear energetically unfavored with respect to the previous ones because of their lower density of intramolecular hydrogen bonding interactions. The structure with lowest energy within this group of conformations (**Xt**) is shown in Figure 7e. In this organization the major stabilizing role is played by N−H··· π interactions, whereas the backbone···backbone interactions are mainly relegated to a five-membered hydrogen bonds, which due to their poor geometry (i.e., ∠N−H···O ≈ 90°) provide much less stability than the seven-and ten-membered ones.

Finally, the β-strand conformation is found in 20th position (**XXt**). This organization appears to be highly disfavored in the gas phase. This structure can be identified as a key one for the formation of fibrils,[44,45] whereas a ΔE value of 6.0 kcal/mol should hinder the adoption of this conformation at room temperature. However, our exploration method did not include the effect of the solvent, which in this particular case can have an important influence not only on the conformational preferences of the peptide but also on its propensity toward aggregation. On the other hand, it has been recently seen[45] that partially folded arrangements, turn and helical like conformation such those characterized as the intermediate energy conformers, play significant roles as aggregate intermediates during early stages of pre − fibril aggregation. This would reduce the energy gap between the preferred arrangement based on turn conformations and the strand conformation required to form long β-sheets.

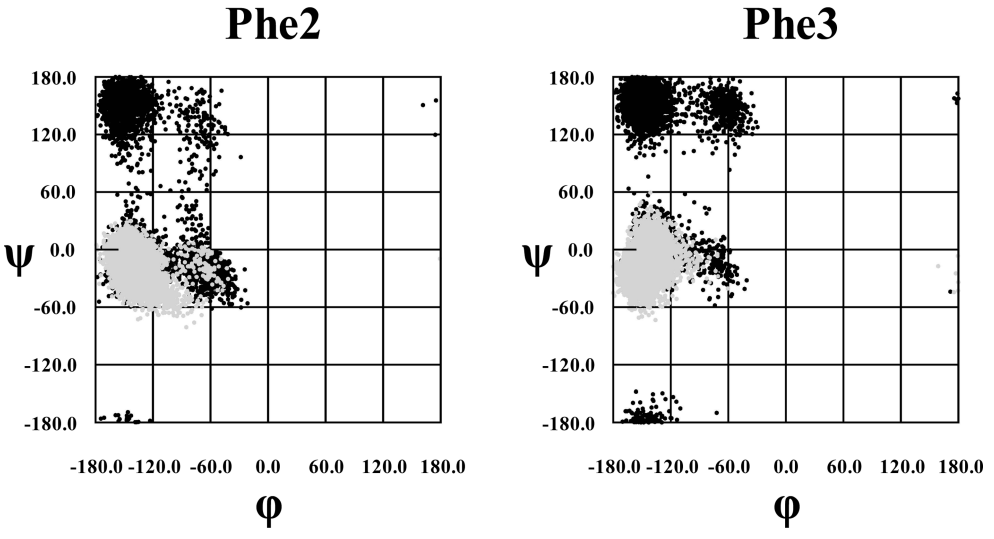

Figure 8. Accumulated Ramachandran plot of the two central Phe residues (label as Phe2 and Phe3) of the FFFF-PEG hybrid amphiphile for 15 ns of simulations. Black dots correspond to the conformations adopted for the first 5 ns, and gray dots refer to the last 15 ns.

dx.doi.org/10.1021/jp2031187 |J. Phys. Chem. B 2011, 115, 8937–8946

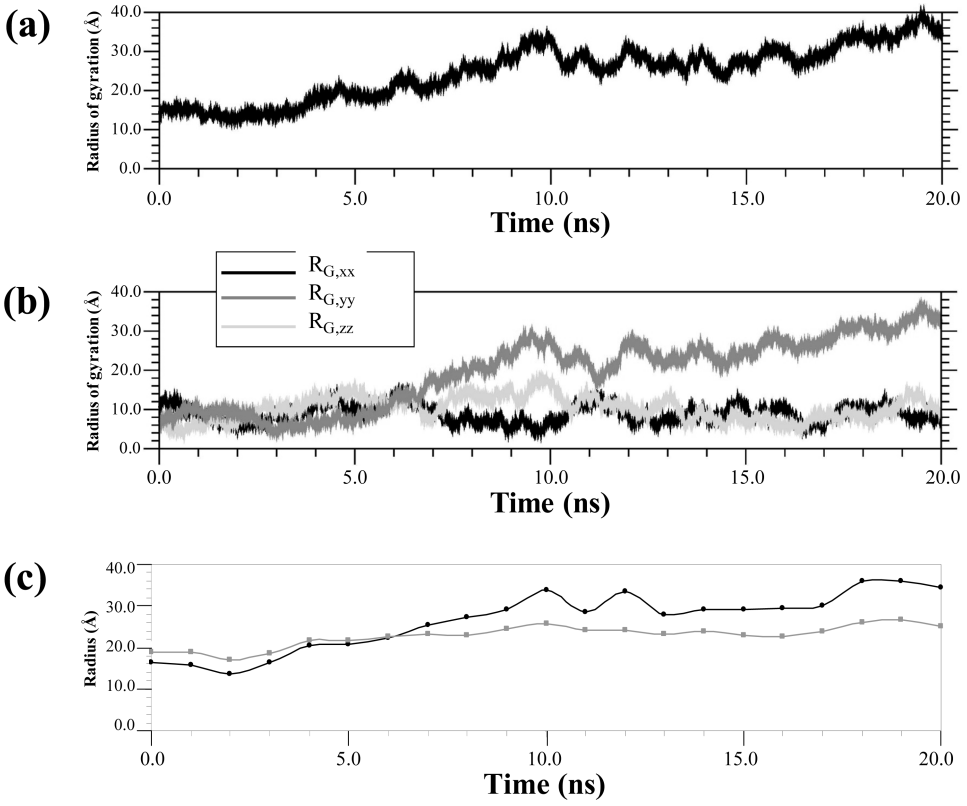

Figure 9. (a) Temporal evolution of the (a) radius of gyration and (b) its three spatial components for the FFFF-PEG hybrid amphiphile. (c) Comparison between the temporal hydrodynamic radius (gray dots) and the radius of gyration (black dots).

Amphiphile FFFF-PEG. The structural organization of the studied amphiphile was characterized in dilute aqueous solution by means of MD simulations. In order to evaluate the influence of both the hydrophilic PEG chain and surrounding solvent molecules, we initially focused on the conformational preferences of the peptide segment, results being compared with those displayed in the previous section for isolated F_4. Figure 8 shows the accumulated Ramachandran plot of the two central residues for the simulated 20 ns. The distribution of both black (first 5 ns of simulation) and gray dots (15 last ns) indicates that the initial conformation, which set around β_{DL} region for each residue, rapidly rearranges to a folded organization. This fast conformational shift and final stabilization of a folded motif is in total agreement with the scenario previously depicted for the isolated peptide, pointing toward an independent behavior of the hydrophobic moiety and the hydrophilic polymer. Comparison between the results provided by the last 15 ns of MD simulation with the minima obtained for F, F_2, and F_4 (Table 1-3) indicates an excellent agreement between the two methodologies. Thus, MD simulations predict that the γ_L, α_L and δ_L folded conformations are the only populated arrangements, which is fully consistent with the minima calculated for the peptides at the B3LYP/6-31G(d) level, especially F_2 and F_4. This feature supports the reliability of the force-field parameters used in this work. Furthermore, results are consistent with experimental observations, which showed that the polymer does not hinder the inner aggregation properties of the peptide (i.e., amyloid like fibrils were formed when the concentration of amphiphile reach the proper value).[6] If the experimentally observed aggregation propensities of F_4 are not altered by the presence of the polymer tails, the conformational independence of the hydrophobic patch when the amphiphile does not form aggregates is a coherent feature.

The structural dynamics of the PEG segment was studied by computing several hydrodynamic properties. Initially, the temporal evolution of the radius of gyration (R_G) was computed for 20 ns of simulation (Figure 9a). The picture drawn by the changes in this property points toward a loss of the initial conformation, which was a compact coil generated using a stochastic methodology.[27,28] The increment in the value of R_G can be attributed to the swallowing of the initial polymer conformation or by a dramatic change in conformational shape. In order to ascertain the relative influence of such two factors, the temporal evolution of the three spatial components of R_G ($R_{G,xx}$, $R_{G,yy}$, and $R_{G,zz}$) has been analyzed (Figure 9b). If the enlargement of R_G is caused by a homogeneous swelling of the initial conformation, the evolution observed for these three spatial components should be similar. However, the results displayed in Figure 9b reflect a different trend: the x and y components remained around the initial values while the z component underwent a drastic increase from around 11 Å to above 35 Å. This behavior must be attributed to a radical conformational change, going from a sphere-like organization (i.e., $R_{G,xx} \approx R_{G,yy} \approx R_{G,zz}$ at the initial conformational) to a partially unfolded state with elongated shape (i.e., $R_{G,xx} \approx R_{G,yy} < R_{G,zz}$).These features are in complete agreement with previous experimental and theoretical works,[46,47] which reported a partially unfolded conformation for PEG in water solution. The conformational changes undergone by the PEG chain are illustrated in Figure 10, which shows selected snapshots recorded during the trajectory.

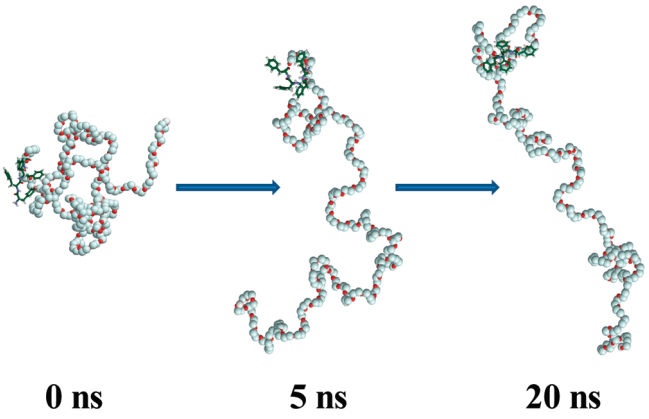

Figure 10. Snapshots of the FFFF-PEG amphiphile taken at the beginning of the simulation and after 5.0 and 20.0 ns of MD.

The calculation of the hydrodynamic radius (R_H) over selected snapshots separated by the same time frame (0.5 ns) reaffirms those previous conclusions. Figure 9c compares the temporal evolution of R_H, which was determined using the program *HYDROPRO* of Garcia de la Torre and co-workers,[48] with the previously computed R_G values. It should be noted that R_H, which should be associated to the effective measure of the hybrid molecule when it is constant diffusion, includes both solvent (hydration) and shape effects.[49] Since most molecules are not perfectly spherical, R_H is smaller than the effective radius (or the rotational radius). As Figure 9c shows, while R_G keeps increasing, the R_H remains steady for the last 15 ns: the averaged value of R_H after that period of time is 23.9 ± 1.4 Å whereas R_G rises to 29.0 ± 4.8 Å for the same period of time. Moreover, if the last 5 ns are compared, the differences are even more marked: while R_H remains stacked around 24 Å (23.7 ± 3.5 Å), R_G reaches values that clearly are above 30 Å (32.0 ± 3.3 Å).

The overall of these results are in excellent agreement with those recently derived by Lee et al.[50] from MD simulations on models of PEG containing 9, 18, 27, and 36 repeating units. Specifically, these authors found that $R_H \approx 0.85R_g$ for low molecular weight PEG in aqueous solution. In the present work the constant of proportionally is 0.74. Consistently, in both cases the constant of proportionally increases with respect to the value deduced from the Kirkwood−Riseman equation for polymer diffusion (0.665),[51] which should be mainly attributed to the waters of hydration. Although the small discrepancy between the constant of proportionally obtained in this work and that reported by Lee et al.[49] should be partially explained by differences in the force-fields, it must be also attributed to the influence of the peptide segment. Thus, the hydrophobicity of the latter is expected to slightly reduce the number of waters of hydration with respect to the pure PEG system of the same molecular weight.

CONCLUSIONS

The results shown in this work have allowed us to depict the conformational preferences of a hybrid amphiphile constituted by a highly hydrophobic peptide and a polymeric tail made of PEG, which conferred the hydrophilic character. The inner conformational properties of the hydrophobic counterpart have been investigated through an extensive and a systematic conformational search using DFT quantum mechanical calculations. A building-up strategy, in which the conformational exploration can be framed to those regions of the energy hypersurface that enclose the lower energy structures, has depicted a scenario that shows a very marked propensity toward arrangements that are the outcome of expanding turn-like conformations throughout the peptide chain. Thus, the most stable arrangements found for F_4 featured regular organizations that either propagated a γ-turn motif from residue one to four, forming a 2.2_7-ribbon structure, or alternated conventional and reverse γ-turns that made up a helical-like arrangement.

On the other hand, in all the studied peptide lengths the aromatic moieties strongly influenced the stability rank of the explored conformations through the formation of backnone···side chain N−H···π interactions. Thus, this feature drives the conformational preferences of the Phe side groups, which are essentially defined by the possibility to form such interactions with the backbone amide groups. The backbone conformation is indirectly responsible for the arrangements adopted by the aromatic side chains, because the conformational freedom of the latter depends on the presence of backbone···backbone intramolecular hydrogen bonds that might hinder the formation of N−H···π interactions.

The conformational preferences of peptide inserted in the amphiphile do not seem to be influenced by the hydrophilic tail. Starting from a completely extended conformation, the peptide rapidly evolves toward a structure very similar to the more stable conformations previously observed in the isolated peptide. The hydrodynamic parameters shown by the hydrophilic counterpart are slightly influenced by the hydrophobic moiety, which affects the number of the number of waters of hydration. In spite of this, it may be considered that both counterparts organize themselves as independent modules, which is in agreement with the reported experimental observations when the amphiphilic material aggregates.[12] In aqueous solution, PEG rapidly unfolds in order to maximize the contacts with the polar solvent and this behavior is analogous to that describe for this polymer when is not part of an amphiphile. This behavior shows that the studied amphiphilic material is capable of independently preserving the inner physical properties of both opposite counterparts and anticipates interesting applications as a self-assembled matrix for encapsulating hydrophobic molecules in polar environments.

AUTHOR INFORMATION

Corresponding Author
*carlos.aleman@upc.edu.

ACKNOWLEDGMENT

Computer resources were generously provided by the Centre de Supercomputació de Catalunya (CESCA). Financial support from Generalitat de Catalunya (research group 2009 SGR 925; XRQTC; ICREA Academia prize for excellence in research to C.A.) is gratefully acknowledged.

REFERENCES

(1) Canalle, L. A.; Lowik, D. W. P. M.; van Hest, J. C. M. *Chem. Soc. Rev.* **2010**, *39*, 329–353.
(2) Klok, H. A. *Macromolecules* **2009**, *42*, 7990–8000.
(3) Klok, H. A. *J. Polym. Sci., A Polym. Chem.* **2005**, *43*, 1–17.
(4) Borner, H. G.; Schlaad, H. *Soft Matter* **2007**, *3*, 394–408.
(5) Lowik, D. W. P. M.; Ayres, L.; Smeenk, J. M.; van Hest, J. C. M. *Adv. Polym. Sci.* **2006**, *202*, 19–52.

(6) Hamley, I. W. *Angew. Chem., Int. Ed.* **2007**, *46*, 8128–8147.
(7) Krysmann, M. J.; Castelletto, V.; Kelarakis, A.; Hamley, I. W.; Hule, R. A.; Pochan, D. J. *Biochemistry* **2008**, *47*, 4597–4605.
(8) Hamley, I. W.; Krysmann, M. J.; Castelletto, V.; Noirez, L. *Adv. Mater.* **2008**, *20*, 4394–4397.
(9) Krysmann, M. J.; Castelletto, V.; Hamley, I. W. *Soft Matter* **2007**, *3*, 1401–1406.
(10) Hamley, I. W.; Krysmann, M. J.; Castelletto, V.; Kelarakis, A.; Noirez, L.; Hule, R. A.; Pochan, D. *Chem.—Eur. J.* **2008**, *14*, 11369–11375.
(11) Hamley, I. W.; Krysmann, M. J.; Newby, G. E.; Castelletto, V.; Noirez, L. *Phys. Rev., E* **2008**, *77*, 062901–062905.
(12) Castelletto, V.; Hamley, I. W. *Biophys. Chem.* **2009**, *141*, 169–174.
(13) Gibson, K. D.; Scheraga, H. A. *J. Comput. Chem.* **1987**, *8*, 826–834.
(14) Flory, P. J., *Statistical Mechanics of Chain Molecules*; Interscience Publishers: New York, 1969.
(15) Dugave, C.; Demange, L. *Chem. Rev.* **2003**, *103*, 2475–2532.
(16) Pal, D.; Chakrabarti, P. *J. Mol. Biol.* **1999**, *294*, 271–288.
(17) Stewart, D. E.; Sarkar, A.; Wampler, J. E. *J. Mol. Biol.* **1990**, *214*, 253–260.
(18) Perczel, A.; Angyán, J. G.; Kajtar, M.; Viviani, W.; Rivail, J.-L.; Marcoccia, J.-F.; Csizmadia, I. G. *J. Am. Chem. Soc.* **1991**, *113*, 6256–6265.
(19) Zanuy, D.; Flores-Ortega, A.; Casanovas, J.; Curco, D.; Nussinov, R.; Aleman, C. *J. Phys. Chem. B* **2008**, *112*, 8692–8700.
(20) Zanuy, D.; Curco, D.; Nussinov, R.; Aleman, C. *Biopolym. (Peptide Sci.)* **2008**, *92*, 83–93.
(21) Zanuy, D.; Flores-Ortega, A.; Jimenez, A. I.; Calaza, M. I.; Cativiela, C.; Nussinov, R.; Ruoslahti, E.; Aleman, C. *J. Phys. Chem. B* **2009**, *113*, 7879–7889.
(22) Revilla-Lo pez, G.; Torras, J.; Nussinov, R.; Aleman C.; Zanuy, D. *Phys. Chem. Chem. Phys.* **2011**, DOI: 10.1039/c0cp02572k
(23) Becke, A. D. *J. Chem. Phys.* **1993**, *98*, 1372–1377.
(24) Lee, C.; Yang, W.; Parr, R. G. *Phys. Rev. B* **1988**, *37*, 785–789.
(25) Hariharan, P. C.; Pople, J. A. *Theor. Chim. Acta* **1973**, *28*, 213.
(26) Frisch, M. J.; Trucks, G. W.; Schlegel, H. B.; Scuseria, G. E.; Robb, M. A.; Cheeseman, J. R.; Scalmani, G.; Barone, V.; Mennucci, B.; Petersson, G. A.; Nakatsuji, H.; Caricato, M.; Li, X.; Hratchian, H. P.; Izmaylov, A. F.; Bloino, J.; Zheng, G.; Sonnenberg, J. L.; Hada, M.; Ehara, M.; Toyota, K.; Fukuda, R.; Hasegawa, J.; Ishida, M.; Nakajima, T.; Honda, Y.; Kitao, O.; Nakai, H.; Vreven, T.; Montgomery, Jr., J. A.; Peralta, J. E.; Ogliaro, F.; Bearpark, M.; Heyd, J. J.; Brothers, E.; Kudin, K. N.; Staroverov, V. N.; Kobayashi, R.; Normand, J.; Raghavachari, K.; Rendell, A.; Burant, J. C.; Iyengar, S. S.; Tomasi, J.; Cossi, M.; Rega, N.; Millam, N. J.; Klene, M.; Knox, J. E.; Cross, J. B.; Bakken, V.; Adamo, C.; Jaramillo, J.; Gomperts, R.; Stratmann, R. E.; Yazyev, O.; Austin, A. J.; Cammi, R.; Pomelli, C.; Ochterski, J. W.; Martin, R. L.; Morokuma, K.; Zakrzewski, V. G.; Voth, G. A.; Salvador, P.; Dannenberg, J. J.; Dapprich, S.; Daniels, A. D.; Farkas, Ö.; Foresman, J. B.; Ortiz, J. V.; Cioslowski, J.; Fox, D. J.; *Gaussian 09*, revision A.1; Gaussian, Inc.: Wallingford, CT, 2009.
(27) Curco, D.; Alemán, C. *J. Chem. Phys.* **2003**, *119*, 2915–2922.
(28) Cortés, J.; Carrión, S.; Curcó, D.; Renaud, M.; Alemán, C. *Polymer* **2010**, *51*, 4008–4014.
(29) Jorgensen, W. L.; Chandrasekhar, J.; Madura, J. D.; Impey, R. W.; Klein, M. L. *J. Chem. Phys.* **1983**, *79*, 926–935.
(30) Cornell, W. D.; Cieplak, P.; Bayly, C. I.; Gould, I. R.; Merz, K. M.; Ferguson, D. M.; Spellmeyer, D. C.; Fox, T.; Caldwell, J. W.; Kollman, P. A. *J. Am. Chem. Soc.* **1995**, *117*, 5179.
(31) Wang, J.; Wolf, R. M.; Caldwell, J. W.; Kollman, P. A.; Case, D. A. *J. Comput. Chem.* **25, 2004**, 1157–1174.
(32) Borodin, O.; Smith, G. D. *Macromolecules* **1998**, *31*, 8396–8406.
(33) Wingera, M.; de Vriesb, A. H.; van Gunsterena, W. F. *Mol. Phys.* **2009**, *107*, 1313–1321.
(34) Alemán, C.; Luque, F. J.; Orozco, M. *J. Comput. Aided Mol. Des* **1993**, *7*, 721.
(35) Phillips, J. C.; Braun, R.; Wang, W.; Gumbart, J.; Tajkhorshid, E.; Villa, E.; Chipot, C.; Skeel, R. D.; Kale, L.; Schulten, K. Scalable Molecular Dynamics with NAMD. *J. Comput. Chem.* **2005**, *26*, 1781–1802.
(36) Berendsen, H. J. C.; Postma, J. P. M.; van Gunsteren, W. F.; DiNola, A.; Haak, J. R. Molecular Dynamics with Coupling to an External Bath. *J. Chem. Phys.* **1984**, *81*, 3684–3690.
(37) Ryckaert, J. P.; Ciccotti, G.; Berendsen, H. J. C. Numerical-Integration of Cartesian Equations of Motion of a System with Constraints - Molecular-Dynamics of N-Alkanes. *J. Comput. Phys.* **1977**, *23*, 327–341.
(38) Jakli, I.; Perczel, A.; Farkas, O.; Hollosi, M.; Csizmadia, I. G. *J. Mol. Struct.* **1998**, *455*, 303–314.
(39) Casanovas, J.; Zanuy, D.; Nussinow, R.; Alemán, C. *J. Org. Chem.* **2007**, *72*, 2174–2181.
(40) Casanovas, J.; Nussinov, R.; Alemán, C. *J. Org. Chem.* **2008**, *73*, 4205–4211.
(41) Casanovas, J.; Jiménez, A. I.; Cativiela, C.; Pérez, J. J.; Alemán, C. *J. Phys. Chem. B* **2006**, *110*, 5762–5766.
(42) Jimenez, A. I.; Ballano, G.; Cativiela, C. *Angew. Chem., Int. Ed.* **2005**, *44*, 396–399.
(43) Reches, M.; Gazit, E. *Science* **2003**, *300*, 625–627.
(44) Görbitz, C. H. *Chem.—Eur. J.* **2001**, *7*, 5153.
(45) Tamamis, P.; Adler-Abramovich, L.; Reches, M.; Marshall, K.; Sikorski, P.; Serpell, L.; Gazit, E.; Archontis, G. *Biophys. J.* **2009**, *96*, 5020–5029.
(46) Yang, X.; Su, Z.; Wu, D.; Hsu, S. L.; Stidham, H. D. *Macromolecules* **1997**, *30*, 3796–3802.
(47) Smith, G. D.; Bedrov, D.; Borodin, O. *J. Am. Chem. Soc.* **2000**, *122*, 9548–9549.
(48) Garcia de la Torre, J.; Huertas, M. L.; Carrasco, B. *Biophys. J.* **2000**, *78*, 719–730.
(49) Strobl, G. R. *The Physics of Polymers Concepts for Understanding Their Structures and Behavior*; Springer-Verlag: Weinheim, Germany, 1996.
(50) Lee, H.; Venable, R.; MacKerell, A. D., Jr.; Pastor, A. W. *Biophys. J.* **2008**, *95*, 1590.
(51) Kirkwood, J. G.; Riseman, J. *J. Chem. Phys.* **1948**, *16*, 565.